Anisotropic mechanical amorphisation drives wear in diamond

Lars Pastewka,[1] Stefan Moser,[1] Peter Gumbsch,[1,2] and Michael Moseler[1,3,4,*]

[1]*Fraunhofer Institute for Mechanics of Materials IWM, Wöhlerstr. 11, 79108 Freiburg, Germany*

[2]*IZBS, Karlsruhe Institute of Technology, Kaiserstr. 12, 76131 Karlsruhe, Germany*

[3]*Freiburg Materials Research Center, Stefan-Meier-Str. 21, 79104 Freiburg, Germany*

[4]*University of Freiburg, Physics Department, Hermann-Herder-Str. 3, 79104 Freiburg, Germany*

Diamond is the hardest material on earth[1]. Nevertheless, polishing diamond is possible with a process that has remained unaltered for centuries and is still used for jewellery and coatings: the diamond is pressed against a rotating disc with embedded diamond grit[2]. When polishing polycrystalline diamond, surface topographies become nonuniform since wear rates depend on crystal orientations[3]. This anisotropy is not fully understood[4] and impedes diamond's widespread use in applications that require planar polycrystalline films, ranging from cutting-tools[5] to confinement fusion[6]. Here, we use molecular dynamics to show that polished diamond undergoes an sp^3-sp^2 order-disorder transition resulting in an amorphous adlayer whose growth rate strongly depends on surface orientation and sliding direction, in excellent correlation with experimental wear rates[7]. This anisotropy originates in mechanically steered dissociation of individual crystal bonds[9]. Similar to other planarisation processes[10], the diamond surface is chemically activated by mechanical means. Final removal of the amorphous interlayer proceeds either mechanically or through etching by ambient oxygen[11].

Scientific investigation of the processes underlying diamond polishing started at the beginning of the last century[2]. Common wisdom among gemstone polishers is that there are "soft" surfaces which exhibit high wear rates, are easy to polish and develop good surface qualities while polishing along "hard" directions is tedious and leads to inferior facets. It was quickly realised that "softness" correlates with crystallographic surface and polishing direction. The $\{110\}$ surface polished in $\langle 100\rangle$ direction (in the following denoted by $\{\mathbf{s}\}\langle\mathbf{d}\rangle = \{110\}\langle 100\rangle$) and the $\{100\}\langle 100\rangle$ surface are soft with the former one being the softest, while polishing $\{100\}\langle 110\rangle$, $\{110\}\langle 110\rangle$ and all directions on the $\{111\}$ surface is hard (see Table 1 for the ordering of experimental wear rates[7]). Similar anisotropy is also seen in the friction coefficient[8]. Initially, the wear anisotropy was explained by removal of small chips of diamond crystals as a result of anisotropic fracture toughness. Using scanning tunneling microscopy, Couto et al.[12] showed that such a process can only account for wear on the hard surfaces. Further investigation revealed that wear particles are mainly amorphous[13], which also contradicts a fracture-based wear mechanism. Recently, atomically thin adlayers of amorphous carbon were detected in wear tracks on nanocrystalline diamond films[14].

In earlier attempts to explain the aforementioned polishing anisotropy, the wear rate was

	soft		hard		
	$\{110\}\langle 100\rangle$	$\{100\}\langle 100\rangle$	$\{110\}\langle 110\rangle$	$\{100\}\langle 110\rangle$	$\{111\}$
Expt.[a]	1	0.9	0.2	0.1	(0.2–0.4[c])
MD[b]	1	0.6	0.5	0.4	< 0.001

TABLE I: Wear rate relative to the softest $\{110\}\langle 100\rangle$ surface/direction. [a] Ref. 7, depth of cut. [b] from fit to the time evolution of the amorphous layer, see text. [c] Wear on the $\{111\}$ surface is due to cleavage. Such processes are not included in our simulations due to the small simulation cell size.

correlated to the diamond's elastic constants[15] or microscopic bonding structure[16]. Both wear models, however, do not go beyond a simple phenomenological treatment. Early classical molecular dynamics (MD) simulations revealed a direction dependence of molecular wear on the $\{111\}$ surface[17]. A similar direction dependence was observed in a first quantum chemical study of a small diamond tip on a diamond $\{110\}$ surface, which showed that bond-breaking requires smaller forces in the soft direction[18]. Despite these efforts a satisfactory understanding of the microscopic wear mechanism is still lacking.

Here, we elucidate the precise microscopic processes underlying diamond polishing using classical MD. Sliding of two unsaturated diamond surfaces with the experimental[4] velocity $v_0 = 30\,\mathrm{m\,s^{-1}}$ and 10 GPa load leads to the gradual destruction of the diamond surfaces. A resulting amorphous interface layer grows steadily during sliding as shown exemplarily for a symmetric pairing of the $\{110\}\langle 100\rangle$ surface in Fig. 1a. This amorphisation can be characterised as an sp^3 to sp^2 order-disorder transition since the amorphous phase consists of roughly 60% sp^2 and 20% sp carbon.

During polishing experiments grit particles rotate in the cast iron matrix until facing a soft orientation to the gemstone[4]. Therefore, pairings of all $\{\mathbf{s}\}\langle\mathbf{d}\rangle$ orientations with either of the two soft orientations are considered in the following. Figure 1b displays the thicknesses of the amorphous interface layer after 20 ns sliding. A clear hierarchy emerges with $\{110\}\langle 100\rangle$ exhibiting the highest and $\{111\}\langle 110\rangle$ the lowest amorphisation rate.

In order to relate the amorphisation to the experimental wear rate we assume a partial removal of the amorphous carbon (a-C) after detachment of the grit particle from the gemstone. Here, we propose two removal mechanisms. First, after simulating separation of the

two sliding partners the last two nanometers of the amorphous layers consists mainly of sp-bonded carbon chains (see Fig. 1c) which are known to be extremely unstable towards CO and CO_2 formation under atmospheric conditions[11]. This mechanism also explains the decrease in wear rate observed with decreasing atmosphere pressure[19]. Second, the diamond grits exhibit sharp edges[4]. In our MD simulation, such an edge scrapes off a small a-C particle during sliding over the a-C (Fig. 1c) in agreement with experiments[13].

Surprisingly, this anisotropic behaviour cannot be detected from the shear-stress which remains at roughly 15 GPa independent of crystallographic orientation suggesting that shear yielding mainly occurs in the amorphous phase. Figure 1d depicts the density, velocity and temperature for a symmetric pairing of the $\{100\}\langle 100\rangle$ surface after 20 ns sliding. The a-C is homogeneous in density and shows small density oscillations close to the a-C–diamond interface reminiscent of fluid layering close to boundaries[20]. In the middle of the a-C layer the velocity shows a Couette profile and fluid-like behaviour. At the interface the a-C phase sticks to the crystal which is similar to fluid flow at large fluid-boundary interaction energies[20]. This fluid-like behaviour is also manifested in a high carbon self-diffusion coefficient in the Couette region. However, the temperature remains as low as 400 K (see Fig. 1c), well below the melting point of diamond at 3500 K (see supplementary section S-I), ruling out an equilibrium melting transition as an explanation for the amorphisation.

A melting transition could be driven by the effective temperature of the sheared glass. However, all definitions of effective temperature collapse at the interface since the carbon atoms are almost immobile and the local shear-rate approaches zero. Also, an Eyring-type[21] description in which the energy barrier towards amorphisation is lowered by the applied shear stress can be ruled out. Mechanical equilibrium dictates a constant shear stress throughout the sample. The drop in chemical potential due to the smaller elastic moduli of the amorphous phase lies below 0.15 eV whereas its cohesive energies is roughly 0.6 eV higher than for diamond (see supplementary section S-II). A similar observation was also made for Lennard-Jones systems[22].

The mechanochemistry of force-driven surface reactions requires formalism beyond Arrhenius activation[9] which is at the heart of all equilibrium thermodynamical processes. Inspection of individual trajectories reveals that the amorphisation happens an atom at a time (see supplementary movies S1 to S3), suggesting a simple microscopic picture involving "pilot"-atoms in the first amorphous adlayer which move slowly over the crystalline surface

(Fig. 2a) and exert time-dependent forces on the terminating surface atoms. Depending on the chemical environment these atoms are able to form a bond which is strong enough[9] to remove the surface atom from its crystalline position leading to an amorphisation event. Assuming that the a-C pilot atoms slide over the diamond surface at a fixed height $a \approx 0.1$ nm (see Fig. 1d) with a velocity $v(a)$, the time evolution of the thickness h of the a-C is given by (see supplementary section S-III for a detailed derivation)

$$\frac{\partial h(t)}{\partial t} = \left(C_{\{\mathbf{s}_1\}\langle\mathbf{d}_1\rangle} P_{\{\mathbf{s}_1\}\langle\mathbf{d}_1\rangle} + C_{\{\mathbf{s}_2\}\langle\mathbf{d}_2\rangle} P_{\{\mathbf{s}_2\}\langle\mathbf{d}_2\rangle}\right) v(a), \tag{1}$$

where $P_{\{\mathbf{s}_i\}\langle\mathbf{d}_i\rangle}$ is the probability for amorphisation of an atom in surface $\{\mathbf{s}_i\}$ by a pilot sliding in direction $\langle\mathbf{d}_i\rangle$. The geometry constants $C_{\{\mathbf{s}_i\}\langle\mathbf{d}_i\rangle}$ are given by $C_{\{\mathbf{s}_i\}\langle\mathbf{d}_i\rangle} = c_{\{\mathbf{s}_i\}} c_{\text{pilot}} l^{\perp}_{\{\mathbf{s}_i\}\langle\mathbf{d}_i\rangle} / n_{\text{a-C}}$. Here, c_{pilot} is the surface density of a-C pilots and $c_{\{\mathbf{s}_i\}}$ the surface density of amorphisable crystalline atoms on surface $\{\mathbf{s}_i\}$. $n_{\text{a-C}}$ is the bulk density in the amorphous phase and $l^{\perp}_{\{\mathbf{s}_i\}\langle\mathbf{d}_i\rangle}$ the distance between two rows of diamond surface atoms that are oriented along the sliding direction $\langle\mathbf{d}_i\rangle$. Employing a position-dependent Herschel-Bulkley model[23] for the viscosity η of the a-C and assuming that η diverges at the diamond interface, the sliding velocity can be calculated as

$$v(a) = \alpha (h + \beta)^{-1} v_0, \tag{2}$$

where the constants α and β depend on the Herschel-Bulkley parameters, the height a of the pilot atoms and the width $w \approx 0.5\,\text{nm}$ of the layered a-C region on the diamond (Fig. 1d). The solution of Eqns. (1) and (2) is given by

$$h(t) = -\beta + \sqrt{(\beta + h(t_0))^2 + 2\left(C_{(\mathbf{s}_1)\langle\mathbf{d}_1\rangle} P_{(\mathbf{s}_1)\langle\mathbf{d}_1\rangle} + C_{(\mathbf{s}_2)\langle\mathbf{d}_2\rangle} P_{(\mathbf{s}_2)\langle\mathbf{d}_2\rangle}\right) \alpha v_0 (t - t_0)}, \tag{3}$$

which is valid for times $t > t_0$ after which the overlap of the layered regions vanishes. This square-root behaviour agrees with experimental observations on the time evolution of wear during polishing of diamond[7].

The $C_{\{\mathbf{s}_i\}\langle\mathbf{d}_i\rangle} P_{\{\mathbf{s}_i\}\langle\mathbf{d}_i\rangle}$ for the different $\{\mathbf{s}_i\}\langle\mathbf{d}_i\rangle$-orientations are obtained by simultaneously fitting the MD results for the pairings shown in Fig. 1b and additional symmetric pairings of the $\{110\}\langle 110\rangle$, $\{100\}\langle 110\rangle$ and $\{111\}\langle 110\rangle$ surfaces to Eq. (3) for $t_0 = 2\,\text{ns}$. As an example, the black solid curves in Fig. 1a shows the resulting fit for a symmetric pairing of the softest $\{110\}\langle 100\rangle$ surface/direction.

In order to compare these results with experiments we compute the amorphisation rate relative to the softest $\{110\}\langle 100\rangle$ surface. The experimental wear rates are taken from

Ref. 7 as the ratios of the depth of wear on the respective surface to the depth on the softest surface. Assuming that the strength of a-C removal mechanisms in Fig. 1c is independent of $\{\mathbf{s}_i\}\langle\mathbf{d}_i\rangle$, this ratio is straightforwardly obtained from the fits to our MD results as $\sqrt{(CP)_{\{\mathbf{s}\}\langle\mathbf{d}\rangle}(CP)^{-1}_{\{110\}\langle100\rangle}}$ in the long-time limit (Table I). While the MD reproduces the experimental ordering of the different surfaces with the exception of the $\{111\}$ surface, the absolute values differ. One needs, however, to keep in mind that our model only describes the amorphisation processes during sliding on the atomic scale where the influence of roughness, the flow of bulk material and description of the final removal of the amorphous layer is excluded. Furthermore, preliminary MD simulations of larger $\{111\}$ surfaces show that these surfaces easily fracture along adjacent $\{111\}$ planes, hinting at a different wear mechanism.

Finally, we address the atomistic origin of the observed anisotropy in $(CP)_{\{\mathbf{s}_i\}\langle\mathbf{d}_i\rangle}$. Since the Cs are not correlated with the wear rates, the Ps must be responsible for the anisotropy (see supplementary section S-III). The Ps are estimated within the pilot-atom picture (Fig. 2a). The left column in Fig. 2b displays a top and side view of the $\{111\}$ surface. The topmost atoms have been saturated by hydrogen in order to mimic bonding to the amorphous phase. The breaking of an orange bond in Fig. 2b leads to the propagation of the topmost orange atom to the first adlayer resulting in an amorphisation event. By stepwise elongating the length of an orange bond while equilibrating the rest of the system, a yield force f_{Y} is determined (see orange force distance curve in Fig. 2c). During the sliding of the a-C pilot layer, the topmost orange atom in Fig. 2b experiences a continuous change of the atomic configuration accompanied by a continuous change of forces f in the orange bonds leading to a bond-breaking event as soon as f_{Y} is exceeded. A rough estimate of the distribution $F(f)$ of forces f is obtained from a sheared bulk a-C sample as a histogram of forces on bonds oriented roughly in the direction of the orange bond (see supplementary section S-IV). The tail of $F(f)$ (Fig. 2d) determines the probability for bond-breaking

$$P = \int_{f_{\mathrm{Y}}}^{\infty} df\, F(f). \tag{4}$$

It is evident from Fig. 2d that P is almost negligible for the $\{111\}$ surface ($P < 10^{-6}$) explaining its pronounced wear resistance. The situation is quite different for the $\{110\}$ surface with its terminating flat-lying zigzag carbon chains (see right column Fig. 2b). During sliding in the soft $\langle100\rangle$ and hard $\langle110\rangle$ direction, the green bond in Fig. 2b breaks and

then the zigzag with the black atom flips in an upright orientation (snapshots in Fig. 2e show this process for the red zigzag chain). This event triggers the sp^3 to sp^2 transition resulting in an characteristic hexagon (cyan atoms in Fig. 2e). Similar to the {111} case, f_Y for the green bond can be calculated (Fig. 2c) providing an estimate $P = 0.05$. For the soft direction, the flipping of the zigzag is the rate limiting step since the cyan hexagon in Fig. 2e is pulled smoothly into the amorphous phase while conserving sp^2 coordination (supplementary movie S2). However, inspection of our MD trajectories shows that amorphisation in the hard direction requires the additional breaking of the red bond (flipped in an upright position - supplementary movie S3) with a larger f_Y and a corresponding smaller $P \approx 0.01$ explaining the smaller wear rates in Table 1.

We believe that mechanochemical amorphisation similar to that found here for diamond occurs on the surface of many tribological systems and contributes to the well-known intermediate tribomutation layer[24] that develops at the sliding interface, sometimes termed "tribomaterial"[25]. We find that the tribomaterial on a diamond surface is chemically active and eases etching. Such surface-activation is likely to also play a crucial role in chemical mechanical processes that are used for the planarisation of dielectrics, semiconductors, metals and composites where the etchant is provided by the slurry[10].

The pilot-atom concept offers a general microscopic explanation of how atoms are carried uphill in energy due to the work performed by the sliding motion (see top panel of Fig. 2a). Like crack propagation and its associated anisotropies[26], the amorphisation obviously is kinetically limited: Time-dependent deformations of the potential energy landscape inhibit the straightforward application of Arrhenius-type laws which depend on the existence of a stationary equilibrium energy barrier. Hence, text-book local-equilibrium thermodynamics breaks down for the description of such sheared systems. Phase-transitions and chemical reactions occurring at the tribointerface under external load will likely lead to new classes of materials and kinds of chemistry yet to be discovered[9].

The uphill process (Fig. 2a) that is at the heart of our wear model has to be distinguished from the formation of amorphous phases due to supercooling[27] or ion bombardment[28,29]. However, we expect materials that show stable amorphous phases in the latter two cases, such as ceramics or metal alloys, to also amorphise during tribological load. The necessary conditions for amorphisation are easily achieved in technical systems such as ball mills or wire saws. Considering the lack of predictive power in heuristic wear laws[30], and the

accompanying lack of basic understanding of machining processes, it is high time for such microscopic wear models.

Methods — The MD simulations were performed as follows. Interatomic forces were computed using the second-generation reactive empirical bond-order potential[31] with a modified cut-off scheme[32]. We specifically tailored this potential to describe tribology of diamond and amorphous carbon by allowing bonds to be broken smoothly, hence avoiding the well-known overestimation of yield forces in interatomic potentials for covalent materials. Previous studies on cracks and amorphous hydrocarbon using this potential have shown good agreement with experiments and density functional theory[32,33].

The atomistic starting configurations were combined from two bulk diamond slabs separated by 9 adatoms to avoid cold-welding resulting in system sizes between 3849 and 6281 atoms. The detailed sizes of the individual slabs are given in supplementary Table S-2. We believe that the influence of the lateral strain introduced due to unavoidable incommensurability of the pairings of different surfaces is small since we observe the same anisotropy in the amorphisation rates of the strain-free pairings of identical surfaces. Atoms in the 3 Å thick top and bottom layers of the sliding systems are held rigid, while the atoms in neighboring 3 Å thick layers are kept at a constant temperature using the Peters-thermostat[34] with a cut-off of 4 Å and a linear weight function. This unusual thermalisation procedure has properties similar to the Langevin thermostat while avoiding contamination of the total shear-stress and the temperature with the thermostat's intrinsic dissipation. The normal pressure is applied using a scheme that has been presented in detail in Ref. 33. Essentially, the upper rigid slab is moved at a constant velocity in the sliding direction, while it is allowed to move damped in the normal direction. The damping constant, and the total mass of the upper slab, is chosen as to minimise finite size effects introduced by the finite periodicity of the system.

Averages in Fig. 1d were collected in 0.1 Å sized bins. The temperature is the average over the kinetic temperatures of the atoms. The force as a function of bond-distance in Fig. 2c has been computed from small periodic samples consisting of 2×2 unit cells in the surface and 3 unit cells in the surface normal direction for the (110) surface. For the (111) surface a $2 \times 3 \times 2$ unit cell has been chosen. While constraining the bond length, a 3 Å bottom layer of atoms was held fixed while the rest of the system was relaxed until the maximum force fell below $0.01\,\mathrm{eV\,\AA^{-1}}$.

Acknowledgments — This work was funded by the BMBF (project OTRISKO) and the Deutsche Forschungsgemeinschaft (Gu 367/30).

Author contributions — L.P., P.G. and M.M. designed the study, developed the amorphisation model and wrote the paper. L.P. and S.M. performed molecular dynamics simulations.

---

* Corresponding author. Email address: michael.moseler@iwm.fraunhofer.de

[1] Field, J. E., *The Properties of Natural and Synthetic Diamond* (Academic Press, London, 1992).

[2] Tolkowsky, W., *Research on the abrading, grinding or polishing of diamond* (DSc thesis, City and Guilds College, University of London, 1920).

[3] El-Dasher, B. *et al.* Crystallographic anisotropy of wear on a polycrystalline diamond surface. *Appl. Phys. Lett.* **88**, 241915 (2006).

[4] Hird, J. R. & Field, J. E. Diamond polishing. *Proc. R. Soc. Lond. A* **460**, 3547–3568 (2004).

[5] May, P. W. Diamond thins films: a 21st-century material. *Phil. Trans. R. Soc. Lond. A* **358**, 473–495 (2000).

[6] Biener, J. *et al.* Diamond spheres for inertial confinement fusion. *Nucl. Fusion* **49**, 112001 (2009).

[7] Wilks, E. M. & Wilks, J. The resistance of diamond to abrasion. *J. Phys. D: Appl. Phys.* **5**, 1902–1919 (1972).

[8] Grillo, S. E., Field, J. E. & van Bouwelen, F. M. Diamond polishing: the dependency of friction and wear on load and crystal orientation. *J. Phys. D.: Appl. Phys.* **33**, 985-990 (2000).

[9] Beyer, M. K. & Clausen-Schaumann, H. Mechanochemistry: The mechanical activation of covalent bonds. *Chem. Rev.* **105**, 2921–2948 (2005).

[10] Krishnan, M., Nalaskowski, J. W. & Cook, L. M. Chemical mechanical planarization: slurry chemistry, materials, and mechanisms. *Chem. Rev.* **110**, 178–204 (2010).

[11] Casari, C. S. *et al.* Chemical and thermal stability of carbyne-like structures in cluster-assembled carbon films. *Phys. Rev. B* **69**, 075422 (2004).

[12] Couto, M. S., van Enckevort, W. J. P., & Seal, M. Diamond polishing mechanisms: An investigation by scanning tunelling microscopy. *Phil. Mag. B* **69**, 621–641 (1994).

[13] van Bouwelen, F. M., Bleloch, A. L., Field, J. E. & Brown, L. M. Wear by friction between

diamonds studied by electron microscopical techniques. *Diam. Rel. Mat.* **5**, 654–657 (1996).

[14] Konicek, A. R. *et al.* Origin of ultralow friction and wear in ultrananocrystalline diamond. *Phys. Rev. Lett.* **100**, 235502 (2008).

[15] van Bouwelen, F. M. Diamond polishing from different angles. *Diam. Rel. Mat.* **9**, 925–928 (2000).

[16] van Bouwelen, F. M. & van Enckevort, W. J. P. A simple model to describe the anisotropy of diamond polishing. *Diam. Rel. Mat.* **8**, 840–844 (1999).

[17] Harrison, J. A. & Brenner, D. W. Simulated tribochemistry: An atomic-scale view of the wear of diamond. *J. Am. Chem. Soc.* **116**, 10399–10402 (1994).

[18] Jarvis, M. R., Pérez, R., van Bouwelen, F. M. & Payne, M. C. Microscopic mechanism for mechanical polishing of diamond (110) surfaces. *Phys. Rev. Lett.* **80**, 3428–3431 (1998).

[19] Hitchiner, M. P., Wilks, E. M. & Wilks, J. The polishing of diamond and diamond composite materials. *Wear* **94**, 103–120 (1984).

[20] Thompson, P. A. & Robbins, M. O. Shear flow near solids: Epitaxial order and flow boundary conditions. *Phys. Rev. A* **41**, 6830–6837 (1990).

[21] Eyring, H. Viscosity, plasticity, and diffusion as examples of absolute reaction rates. *J. Chem. Phys.* **4**, 283–291 (1936).

[22] Butler, S. & Harrowell, P. Factors determining crystal-liquid coexistence under shear. *Nature* **415**, 1008–1011 (2002).

[23] Herschel, W. H. & Bulkley, R. Konsistenzmessungen von Gummi-Benzollösungen. *Kolloid Z. Z. Polym.* **39**, 291–300 (1926).

[24] Persson, B. N. J. *Sliding Friction* (Springer, Berlin, 2001).

[25] Rigney, D. A. & Karthikeyan, S. The evolution of tribomaterial during sliding: A brief introduction. *Tribol. Lett.* **39**, 3–7 (2010).

[26] Gumbsch, P. & Cannon, R. M. Atomistic aspects of brittle fracture. *MRS Bulletin* **25**, 15–20 (2000).

[27] Angell, C. Formation of glasses from liquids and biopolymers. *Science* **267**, 1924–1935 (1995).

[28] Williams, J. S. Materials modification with ion beams. *Rep. Prog. Phys.* **49**, 491–587 (1986).

[29] Moseler, M., Gumbsch, P., Casiraghi, C., Ferrari, A. C. & Robertson, J. The ultrasmoothness of diamond-like carbon surfaces. *Science* **309**, 1545–1548 (2005).

[30] Meng, H. C. & Ludema, K. C. Wear models and predictive equations: their form and content.

Wear **181-183**, 443–457 (1995).

[31] Brenner, D. W. *et al.* A second-generation reactive empirical bond order (REBO) potential energy expression for hydrocarbons. *J. Phys.: Condens. Matter* **14**, 783–802 (2002).

[32] Pastewka, L., Pou, P., Pérez, R., Gumbsch, P. & Moseler, M. Describing bond-breaking processes by reactive potentials: Importance of an environment-dependent interaction range. *Phys. Rev. B* **78**, 161402(R) (2008).

[33] Pastewka, L., Moser, S. & Moseler, M. Atomistic insights into the running-in, lubrication, and failure of hydrogenated diamond-like carbon coatings. *Tribol. Lett.* **39**, 49–61 (2010).

[34] Peters, E. A. J. F. Elimination of time step effects in DPD. *Europhys. Lett.* **66**, 311–317 (2004).

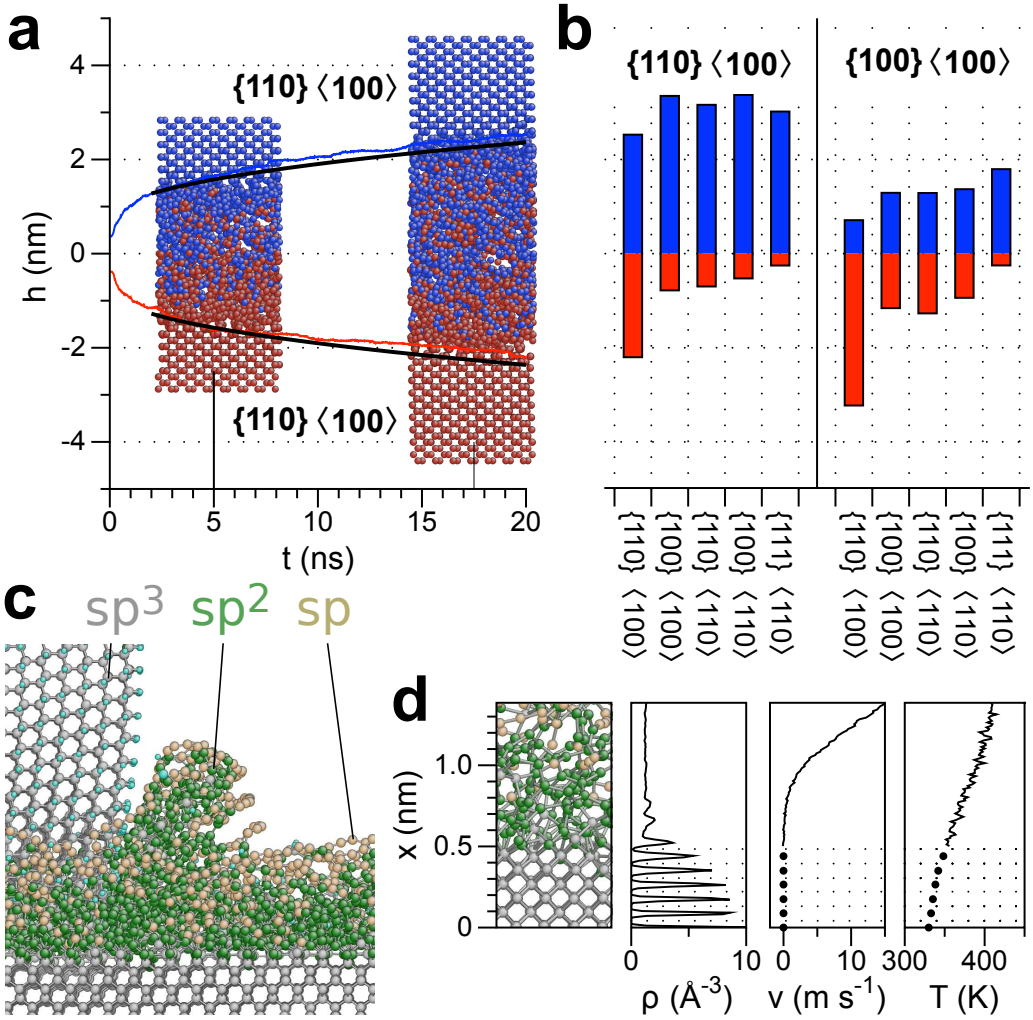

FIG. 1: Molecular dynamics simulation of diamond polishing. **a**, Time evolution of the thickness of the amorphous layer for a symmetric pairing of the $\{110\}\langle 100\rangle$ surface. The insets show snapshots after 5 ns and 17.5 ns. Colours mark whether an atom stems from the top or bottom slab of diamond. Black solid lines: model results as described in the text. **b**, Final thickness of the amorphous layer after 20 ns for various surface pairings. **c**, A diamond grit edge piles up an amorphous carbon particle. **d**, Snapshot of the $\{100\}\langle 100\rangle$ surface after 20 ns of sliding. The density, velocity and temperature profile is a 1 ns average at 20 ns. Colours in **c** and **d** indicate atomic coordination.

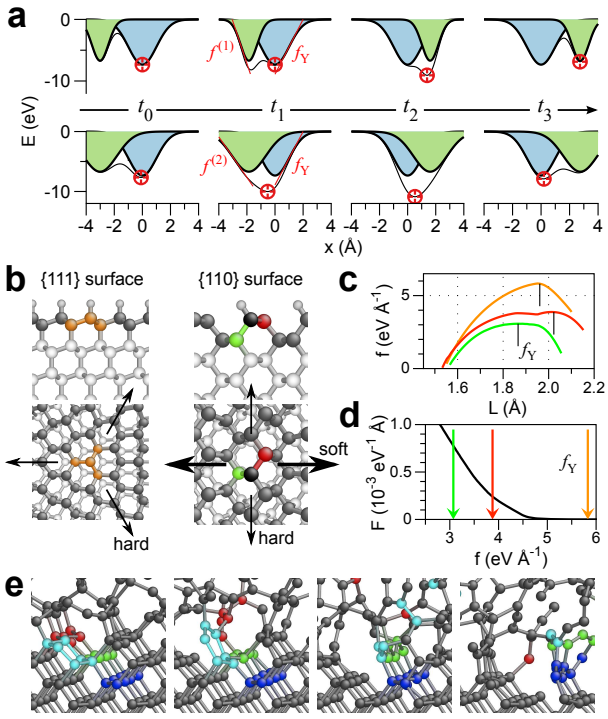

FIG. 2: Microscopic origin of the anisotropy. **a**, Illustration of the "pilot" atom concept. Initially, an atom (marked by the red circle) resides on a crystal position (marked by the blue stationary potential well). During sliding, an a-C atom approaches from the left and forms a bond to the crystal atom (represented by the green moving potential well). Depending on the maximum slopes of the potential wells ($f^{(1)}$, $f^{(2)}$, f^{Y}), the crystal atom follows the a-C pilot atom (first row, $f^{(1)} > f_{\mathrm{Y}}$) or remains on its initial lattice site (second row, $f^{(2)} < f_{\mathrm{Y}}$). **b**, Sketches of the diamond {111} and {110} surfaces. The hard and soft polishing directions are marked by thin and thick arrows, respectively. Bonds that break during an amorphisation event are in orange, red and green. Large spheres represent carbon and small spheres terminating hydrogen. While on the {111} surface the topmost orange atoms are connected to the amorphous phase, on the {110} only every second atom forms a bond to a-C (see panel **e**). Therefore, the hydrogen termination on the {110} surface is chosen to give chemical environments similar to the MD simulations. **c**, Constraint force as a function of bond-length for the bonds that are colour-coded in panel **a**. The maximum force defines the critical yield force f_{Y}. The red curve shows the yield function for the red {110} bond after flipping in an upright position. Note that $1\,\mathrm{eV\ \AA^{-1}} \approx 1.6\,\mathrm{nN}$. **d**, Probability distribution of force fluctuations in the a-C (black curve). The coloured arrows mark the yield forces for the different bonds in panel **a**. **e**, The amorphisation process for {110}⟨100⟩. Zigzag chains in three different layers are red, green and blue.